ARTICLE

Two-Dimensional Infrared Spectroscopy of the Photoproduct of π-Cyclopentadienyliron Dicarbonyl Dimer[†]

Fan Yang[a], Peng-yun Yu[a,b], Ji-pei Shi[a,b], Juan Zhao[a], Xue-mei He[a,b], Jian-ping Wang[a*]

a. Beijing National Laboratory for Molecular Sciences; Molecular Reaction Dynamics Laboratory, Institute of Chemistry, Chinese Academy of Sciences, Beijing 100190, China
b. University of Chinese Academy of Sciences, Beijing 100049, China

(Dated: Received on November 16, 2013; Accepted on December 2, 2013)

Equilibrium photoproduct of π-cyclopentadienyliron dicarbonyl dimer $[CpFe(CO)_2]_2$ in non-polar solvent carbon tetrachloride (CCl_4) is investigated using time-resolved 2D IR spectroscopy. One of the several possible visible-light-driven photoreaction pathways is confirmed and the product is found to contain a di-carbonyl group that exhibits quantum beating between two equivalent transitions in time-resolved 2D IR spectra, which turns out to be the anti-symmetric and symmetric stretching of the terminal carbonyl stretching modes of $CpFe(CO)_2Cl$. This is the main product and its reaction pathway involves radical formation, followed by chloride addition. Quantum-chemistry computations support these experimental results. Our results indicate that 2D IR method can be used to identify *in situ* structures and dynamics of chemical species involved in condensed-phase chemical reactions.

Key words: Organometallic compound, Photoproduct, Carbonyl stretch, 2D IR spectroscopy

I. INTRODUCTION

It is widely known that condensed phase chemical reactions usually have multi-paths and multi-products, which means complicated reaction mechanisms. Product identification can usually be carried out by using analytical methods that are either mass-sensitive or structure-sensitive. Among the latter, nuclear magnetic resonance (NMR) method is superior because it has atomic level of structural resolution. For this reason, NMR spectroscopy is commonly used in chemical-synthesis laboratories for structural identification. On the other hand, vibrational method such as infrared (IR) absorption spectroscopy, also has structural sensitivity at the level of chemical-bond. This is because the smallest infrared chromophore is a two-atom stretch that is ubiquitous in any molecule. Thus the structural sensitivity of the IR method is comparable to that of the NMR method.

Indeed, linear IR has been used effectively to identify stable chemical species in condensed phases. In particular, femtosecond two-dimensional infrared (2D IR) spectroscopy [1−10] has made IR method a even more powerful tool for examining the structures and their distributions of equilibrium species [11, 12], and the chemical species that can undergo equilibrium exchange reactions [13, 14]. Transient and non-equilibrium species generated from photoreactions can also be characterized [15].

Small organometallic compounds are very useful models for condensed-phase molecular systems [16, 17]. In particular, metal carbonyl (C≡O) group containing organometallic compounds can be used as effective structural probes for vibrational spectroscopic applications. The CO containing systems have been studied in recent years by using the 2D IR spectroscopy, in order to understand the structures and dynamics of the molecular systems themselves, *e.g.* $Rh(CO)_2acac$ [18−21], in transition-state involving chemical reactions [14, 22, 23], in dye sensitizers for solar energy conversion [24], as well as in the application of CO releasing molecule (CORM) [25, 26].

$[CpFe(CO)_2]_2$, π-cyclopentadienyliron dicarbonyl dimer, a well-known dinuclear organometallic complex, has provided remarkably rich and complex organometallic structural chemistry and photochemistry that lead to a variety of fundamentally interesting products [27]. For $[CpFe(CO)_2]_2$ itself, because the rotation about the Fe−Fe bond can not easily occur, the two terminal CO groups can be arranged in *cis* or *trans* positions with respect to the π-cyclopentadienyl (Cp, π-C_5H_5). Like many metal carbonyl complexes that contain formal metal−metal single bonds, $[CpFe(CO)_2]_2$ has two distinct photochemical channels, namely homolysis of the metal−metal bond to form two 17-electron $CpFe(CO)_2$ radicals, which was first sug-

[†]Part of the special issue for "the Chinese Chemical Society's 13th National Chemical Dynamics Symposium".
*Author to whom correspondence should be addressed. E-mail: jwang@iccas.ac.cn, Tel.: +86-10-62656806, FAX: +86-10-62563167

gested to contain a highly symmetric triply bridged structure on the basis of nearly simultaneous investigations by Rest and coworkers [28] and by Winterton and coworkers [29]. The other pathway is to break the bridged CO so as to give at least two isomeric species. Numerous mechanistic studies have led to the proposal of unusual species as intermediates in the photochemical transformation. For example, an early ultrafast study by Hochstrasser *et al.* showed that bands of both the *cis* and *trans* isomers of $[CpFe(CO)_2]_2$ were bleached to give new features in the terminal carbonyl region that evolved over 100 ps to the band that is characteristic of the $(\eta_5\text{-}C_5H_5)Fe(CO)_2$ radical [27].

We have previously examined vibrational and rotational dynamics of $[CpFe(CO)_2]_2$ in CH_2Cl_2 using transient infrared pump-probe method [30]. A recent 2D IR study showed that in $[CpFe(CO)_2]_2$ vibrational energy redistribution (IVR) exists [23]. In this work, we examine the structural and dynamics of the photoproduct of $[CpFe(CO)_2]_2$ in a nonpolar solvent (CCl_4) using the FTIR and 2D IR spectroscopies. A reaction product under steady-state room light illumination of $[CpFe(CO)_2]_2$ is obtained. We find this product is stable for at least 24 h in a concealed container as prepared. We then carry our FTIR and 2D IR measurements. Waiting-time-dependent 2D IR method is used to positively identify the key signature of the photoproduct that is found to be $CpFe(CO)_2Cl$. The structural dynamics and intramolecular IVR pathways of this photoproduct are also examined.

II. MATERIALS AND METHODS

A. Sample and 1D IR experiments

$[CpFe(CO)_2]_2$ was purchased from TCI (96% purity) and used without further purification. $CpFe(CO)_2$ dimer was dissolved in CCl_4 with insoluble precipitate removed by filtration. The sample solution showed a pellucid wine red color. The concentration was estimated to be 30 mmol/L. The solution was filled into an IR sample cell composed of two 2-mm thick calcium fluoride windows separated by a 50-μm Teflon spacer. The IR spectra of $[CpFe(CO)_2]_2$ in the terminal C≡O stretching frequency region were collected using a Nicolet 6700 FT-IR spectrometer (Thermo Electron) with 1-cm^{-1} resolution.

Furthermore, the prepared $[CpFe(CO)_2]_2$-CCl_4 solutions in sealed bottle and/or IR cells were irradiated using white-light (with power of ca. 1 W) for several hours. A series of IR spectra were collected to track the photoreaction process for 4 h with an interval of 10 min for the first 3 h and 30 min for the last hour. During this process the color of solution turned from wine red to orange. Photoreaction was found to complete after 4 h and the photoproduct was stable in CCl_4 for at least 24 h, thus allowing linear IR and 2D IR spectra to be taken. All the IR measurements were carried out at room temperature (22 °C).

The photoreaction product was analyzed using mass spectroscopy. Briefly, the photoproduct solution was diluted four times by ethanol, and the mass spectrum was immediately measured using a Thermo Fisher LTQ mass spectrometer (Thermo Scientific Inc., San Jose, CA) in positive mode. The mass spectrum was found to be dominated by a main species with m/z=230, which was found to be the hydrated complex $[C_5H_5Fe(CO)_2ClH_2O]^+$. It showed an isotope peak at m/z=232 with 1/3 intensity of the former, suggesting the presence of chloride and the species to be $[C_5H_5Fe(CO)_2{}^{37}ClH_2O]^+$. Thus the main product was believed to be $CpFe(CO)_2Cl$. The hydration was believed to take place during the electrospray ionization process.

B. 2D IR experiments

A home-build 2D IR spectrometer was used to collect 2D IR spectra. The experimental apparatus has been described in detail elsewhere [31]. As a result, only a brief description will be given here. Briefly, a commercial ultrafast Ti:Sapphire laser amplifier generated 1-kHz, 800-nm, 3-mJ, sub 35-fs pulse was used to pump an optical parametric amplifier using up to one third of the output energy of the laser amplifier. The signal and idler pulses in near IR region produced by the OPA were used to produce a 70-fs, 5-μJ mid-IR pulse by difference frequency mixing in a 0.5-mm thick type-II $AgGaS_2$ crystal. The obtained IR pulse was tuned to a center frequency at 1980 cm^{-1} with FWHM of ca. 250 cm^{-1}. The mid-IR pulse was then split into three excitation beams (ca. 400 nJ each) for photon echo experiment, and a much weaker beam as the local oscillator (LO) for heterodyned detection, which provided a phase reference for the echo signal. The time-order of the four pulses was varied by changing their relative delays. The delay time between the first and second pulses ($\mathbf{k}_1$ and $\mathbf{k}_2$) is the coherence time τ and between the second and third pulses is the waiting time T. The three excitation pulses were focused on the liquid sample by a parabolic mirror, and the emitted third-order nonlinear signal (echo) was monitored in the $-\mathbf{k}_1+\mathbf{k}_2+\mathbf{k}_3$ phase-matching direction, whose time axis was the same as the $\mathbf{k}_3$ pulse. Four laser pulses were set to vertical polarization for parallel 2D IR measurement. An IR monochromator equipped with a 64-element liquid nitrogen-cooled mercury-cadmium-telluride (MCT) array detector was used to collect the combined echo/local oscillator pulses using the IR spectral interferometry approach, in which the local oscillator precedes the echo signal. Numerical FT along the τ-axis yielded the frequency domain 2D IR spectra. In the experiments, τ was scanned typically in a 2.5-ps time window at the step of 5 fs, for a fixed T, to produce a 2D IR spectrum. A series of T-dependent 2D IR spectra were collected.

DOI:10.1063/1674-0068/26/06/721-728

TABLE I Linear IR fitting parameters of $[CpFe(CO)_2]_2$ reactant and its photoproduct $CpFe(CO)_2Cl$ in CCl_4 with Lorentzian function.

Species	Mode	$[CpFe(CO)_2]_2$		$CpFe(CO)_2Cl$	
	assignment	Peak position/cm^{-1}	Lorentzian width/cm^{-1}	Peak position/cm^{-1}	Lorentzian width/cm^{-1}
cis	ss	2004.3	7.3	2055.0	5.9
	as	1965.0	6.8	2011.5	7.8
trans	as	1959.0	11.5		

as=anti-symmetric stretching, ss=symmetric stretching.

Equally weighted rephasing and non-rephasing 2D IR spectra yield the so-called pure absorptive spectra. The projection of the 2D IR spectra on the detection frequency, in comparison with the IR pump-probe signal that was collected using $\mathbf{k}_3$ (pump) and an attenuated $\mathbf{k}_1$ (probe), was used to phase the 2D IR signals.

The vibrational population relaxation time constants were measured with the femtosecond IR pump-probe experiment at the magic angle (54.7°) condition. Perpendicular polarization pump-probe experiment was also carried out in order to compute the anisotropy signal. All nonlinear IR measurements were carried out at room temperature (22 °C).

C. Quantum chemical calculations

The vibrational properties of $[CpFe(CO)_2]_2$ and $CpFe(CO)_2Cl$ in gas phase were examined at the level of the density functional theory (DFT). The calculations were performed using B3LYP functional with the 6-31++G** basis set for the carbon, oxygen, hydrogen, and chlorine atoms and the sdd pseudopotential for the iron atom. Harmonic vibrational transition frequencies and intensities, in particular those for the two terminal carbonyl (C≡O) stretches were obtained. The computation was carried out using Gaussian 03 [32].

III. RESULTS AND DISCUSSION

A. Linear IR spectra and band assignment

Figure 1 shows the linear FTIR spectra of the $[CpFe(CO)_2]_2$ and its photoreaction product $CpFe(CO)_2Cl$ in CCl_4 at different lengths of time upon room-light irradiation. For $[CpFe(CO)_2]_2$ reactant in CCl_4 without light irradiation, the two peaks are located at 2004.3 and 1959.0 cm^{-1}, which can be assigned to the *cis* and *trans* forms of the non-bridged C≡O stretching modes respectively [30]. Thus the compound exists as an equilibrium mixture of two structurally isomeric molecular forms. It is seen that as the photoreaction proceeds, the two peaks first decrease then disappear almost completely, and two new absorption bands exclusively appear at 2011.5 and 2055.0 cm^{-1} in approximately equal populations (solid line), with a frequency separation to be 43.5 cm^{-1}. These two new appearing bands are most probably due to terminal C≡O stretching modes that come from $CpFe(CO)_2$ monomer-like species, with quite high quantum yield. It turns out that the reaction product is $CpFe(CO)_2Cl$, a conclusion mainly drawn from our 2D IR results (see below). The peaks of the reactant and product of $[CpFe(CO)_2]_2$ in CCl_4 can be fitted using Lorentzian functions and the fitting parameters are listed in Table I. For the reactant, the fitting correlation coefficient for the two peaks together is 0.99617, and for the photoproduct, the coefficient is 0.99793. As is shown, full width at half maximum (FWHM) of the low-frequency band is a little broader than that of the high-frequency one, indicating that the two components, which are the anti-symmetric and symmetric C≡O stretching modes, are influenced by solvent differently.

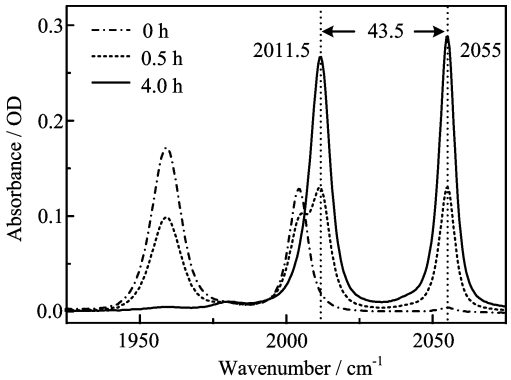

FIG. 1 Linear IR spectra of the C≡O stretch of $[CpFe(CO)_2]_2$ (dot and dashed lines) and its reaction product (solid line) in CCl_4 as a function of light irradiation time.

B. Quantum chemistry computations

The optimized structure $CpFe(CO)_2Cl$ is shown in Fig.2, in comparison with the two structures of $[CpFe(CO)_2]_2$. The normal-mode frequency and intensity for the harmonic vibrations of the symmetric and antisymmetric C≡O stretching modes are computed and the results are listed in Table II. For $CpFe(CO)_2Cl$, the frequency of the symmetric stretching of the two

DOI:10.1063/1674-0068/26/06/721-728

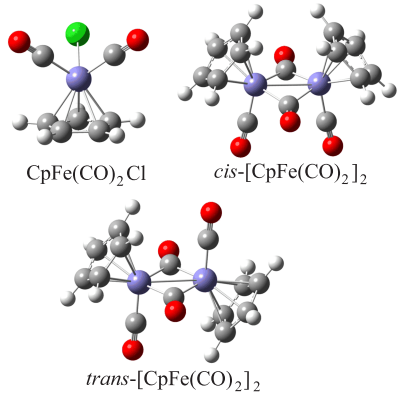

FIG. 2 Optimized structures of $CpFe(CO)_2Cl$ and $[CpFe(CO)_2]_2$ in gas phase.

TABLE II Harmonic frequencies (ω_i) and the IR intensities (I) of the two C≡O stretching vibrational modes of $CpFe(CO)_2Cl$ and $[CpFe(CO)_2]_2$ in gas phase.

	Mode	ω_i/cm^{-1}	I/(km/mol)
$CpFe(CO)_2Cl$	ss	2133.1	690.8
	as	2100.9	783.6
cis-$[CpFe(CO)_2]_2$	ss	2081.9	1485.0
	as	2044.9	205.0
trans-$[CpFe(CO)_2]_2$	ss	2055.1	0.005
	as	2041.5	1557.0

C≡O bonds is higher than that of the antisymmetric stretching, and the frequency shift between the two vibrational modes is 32.2 cm^{-1}. The intensity of the antisymmetric stretching mode is higher than that of the symmetric stretching mode. It can be seen that the frequency and intensity of the symmetric and antisymmetric forms are consistent with the peaks of FTIR spectra. However, it is noted that the quantum chemistry computational results are only used to guide experimental data interpretation. A perfect match between computation and experiment can not be easily reached, even using more sophisticated theoretical method.

On the other hand, $[CpFe(CO)_2]_2$ has two stable conformations, the *cis* and *trans* conformations (Fig.2), named in terms of the positions of two terminal carbonyl groups. There are two C≡O stretching modes, anti-symmetric stretching mode and symmetric stretching modes, for both *cis* and *trans* conformations. In both conformations, the frequency of the symmetric stretching of the two C≡O bonds is higher than that of the anti-symmetric stretching, and the frequency separation between the two modes (37 cm^{-1}) in the *cis* conformation is larger than that (13.6 cm^{-1}) in the *trans* conformation. This indicates that the coupling between the two C≡O stretching modes in the *cis* conformation is stronger than that in the *trans* conformation. We also can see that in the *cis* conformation, the transition intensity of the symmetric stretching mode is stronger than that of the antisymmetric stretching mode; however, the symmetric stretching is an infrared-inactive mode in the *trans* conformation.

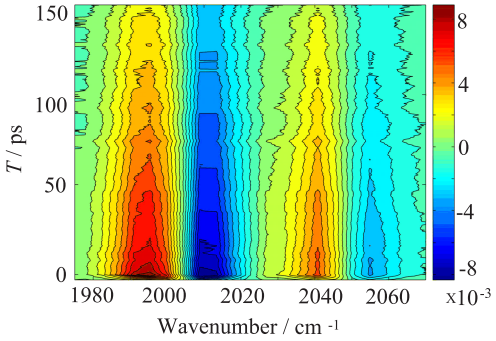

FIG. 3 Magic-angle pump-probe spectra of the photoproduct of $[CpFe(CO)_2]_2$ in CCl_4 in the terminal C≡O stretching region.

C. Transient pump-probe spectra

The magic-angle broadband pump-broadband probe spectra of $CpFe(CO)_2Cl$ at the magic polarization are given in Fig.3. The spectra were measured from 0 to 150 ps delay at 0.3 ps step. There are two pairs of transient signals. The negative (blue) and positive (red) signals arise from the 0→1 (*i.e.*, v=0→v=1 where v is the vibrational quantum number) and 1→2 vibrational transitions respectively. The high-frequency pair is due to the symmetric form of the two nearby C≡O stretches while the low-frequency pair is mainly due to the antisymmetric form. Their negative peaks are very close to, but different from those observed in FTIR (2055.0 and 2011.5 cm^{-1}) because of the overlap between the bleach and absorption signals. Both red and blue signals of the low-frequency component show somewhat broader spectral linewidth than those of the high-frequency component, which is consistent with the FTIR results.

The transient intensity of the high frequency component is lower than that of the low frequency component in pump-probe spectra. Because their linear IR spectra show similar intensity, this result suggests that the vibrational anharmonicity for the high-frequency symmetric vibration is smaller than that of the low-frequency anti-symmetric vibration. Furthermore, a slice of pump-probe spectrum can be used to obtain the anharmonicities for the two transitions, which are found to be 16.8 and 18.4 cm^{-1} respectively for the high-frequency and low-frequency components.

In order to reveal the vibration relaxation dynamics of the photoproduct of $[CpFe(CO)_2]_2$, the vibrational lifetime was extracted from the time-dependent pump-probe spectra. Figure 4 shows the vibration relaxation dynamics obtained using the bleaching signals from the time-dependent magic-angle pump-probe data shown in Fig.3. The relaxation has not yet decayed completely

DOI:10.1063/1674-0068/26/06/721-728

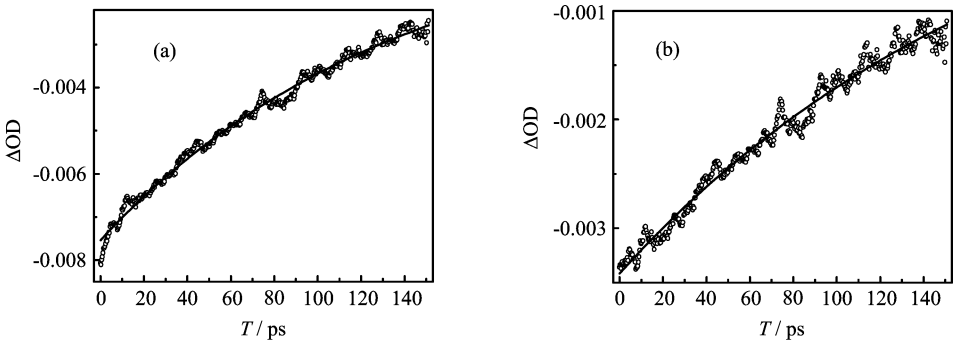

FIG. 4 Life time determinations using the bleach recovery for (a) the antisymmetric and (b) the symmetric C≡O stretching modes of the photoproduct of $[CpFe(CO)_2]_2$ in CCl_4.

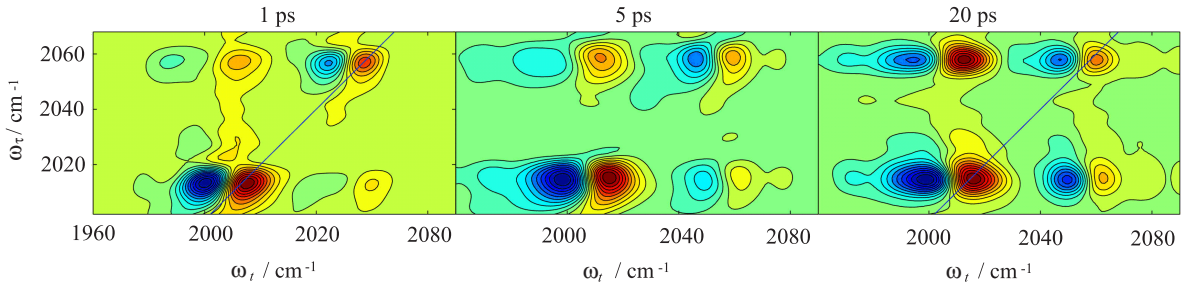

FIG. 5 Waiting-time resolved absorptive 2D IR spectra of the photoproduct of $[CpFe(CO)_2]_2$ in CCl_4 at different waitting time. The real parts of the absorptive spectra are shown.

in the range of time up to 150 ps, however, the results showed that the ss- and as-component decay differently (136.9 ps *vs.* 188.5 ps). The vibrational lifetimes are fitted using single exponential function, and the results are given in Table III. It is seen that the population relaxation time constant T_1 of the two C≡O stretching modes in $CpFe(CO)_2Cl$ are much longer than those observed in $[CpFe(CO)_2]_2$ reactant (ca. 22−27 ps, not shown) in the same solvent, or in CH_2Cl_2 (ca. 20 ps), as reported earlier [30]. We believe this is mainly due to the molecular structure effect, which plays an important role in the IVR process. Solvent effect, on the other hand, is not so critical because the T_1 values are quite similar in CH_2Cl_2 and CCl_4 for $[CpFe(CO)_2]_2$.

In addition, using magic-angle data and perpendicular data, the anisotropy relaxation dynamics are also obtained. The rotation $r(T)$ can be written as a function of the $I_m(T)$ and $I_v(T)$, as follows:

$$r(T) = 1 - \frac{I_v(T)}{I_m(T)} \tag{1}$$

where T is the waiting time. $I_m(T)$ and $I_v(T)$ represent the pump-probe intensity measured with magic and perpendicular relative polarizations, respectively. The data are not given here but the fitting results are listed in Table III. It is observed that the molecular orientational relaxation time constants determined from the antisymmetric stretching and symmetric stretching modes are quite similar (8.8 ps), which is slightly faster than that of the same molecule in CH_2Cl_2 (ca. 10 ps) [30].

TABLE III The vibrational relaxation dynamics and the rotational dynamics fitted to single exponential functions for photoproduct of $[CpFe(CO)_2]_2$ in CCl_4, probed at their IR absorption peak positions.

Frequency/cm^{-1}	A/%	T_1/ps	r_0	$r_{\rm offset}$	$\tau_{\rm or}$/ps
2011	100	136.9±4.2	0.28	0.15	8.8±0.9
2055	100	188.5±11.4	0.14	0.09	8.8±2.0

A is the amplitude, $\tau_{\rm or}$ is the rotational relaxation time, r_0 and $r_{\rm offset}$ are initial and final amplitudes of anisotropy.

D. 2D IR spectra

We obtain the 2D IR spectra of photoproduct of $[CpFe(CO)_2]_2$ in CCl_4 at different T values, which are shown in Fig.5. Each spectrum consists of two diagonal and off-diagonal peaks. The positive (red) and negative (blue) diagonal peaks in the spectra arise from the 0→1 and 1→2 vibrational transitions, respectively. Here the 1→2 transition appears to be shifted along the ω_t axis due to vibrational anharmonicity of the normal mode, *i.e.*, the energy gap of the 1→2 is less than that of the 0→1 transition. The diagonal vibrational anharmonicity for the high-frequency symmetric and low-

DOI:10.1063/1674-0068/26/06/721-728

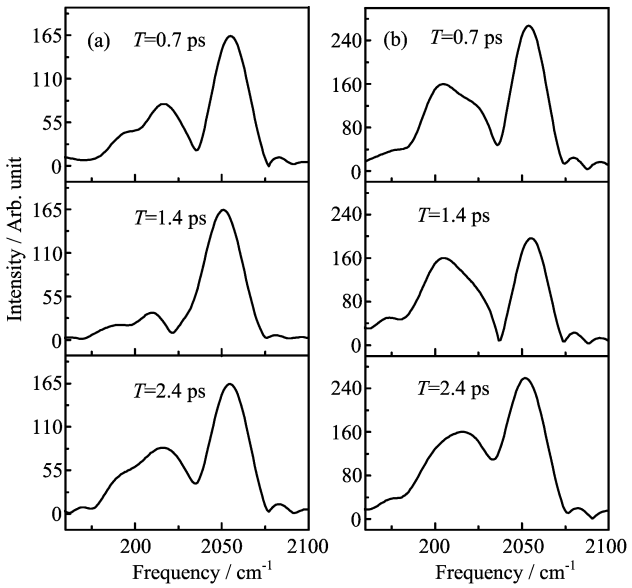

FIG. 6 Slice spectra of the rephasing (a) and non-rephasing (b) magnitude 2D IR spectra at ω_τ=2055 cm^{-1}.

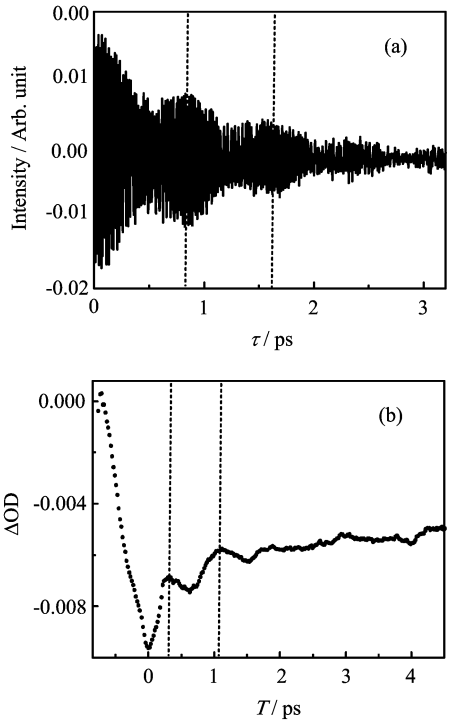

FIG. 7 (a) The signal trace from non-rephasing spectra as function of coherence time τ at ω_t=2011 cm^{-1}. (b) A blow-up of the pump-probe trace at 2011 cm^{-1} with a period of 760 fs.

frequency anti-symmetric vibrations are obtained from Fig.5, which are about 13 and 16 cm^{-1}, respectively.

It is observed that the 2D IR spectra are elongated along the diagonal at early T value. As T increases, the 2D spectra become more vertically tilted for both the 0→1 and 1→2 transitions. The change of the diagonal 2D spectra is due to the vibrational spectral diffusion [33], that is related to the frequency-frequency time-correlation function [34]. It is also observed that the off-diagonal signals increase as a function of the T time, indicating that the intramolecular vibrational energy transfer exists between the symmetric and anti-symmetric vibrations modes of $CpFe(CO)_2Cl$. Treating IVR as an equilibrium process the timescales for both the backward and forward transfer of energy can be obtained. However, this is beyond the scope of this work [23].

E. The observation of quantum beating of a pair of coupled vibrators

Figure 6 shows the slice spectra of both rephasing and non-phasing magnitude 2D IR spectra. The waiting times for these spectra are chosen to roughly coincide with a period of 760 fs. In the rephasing spectra the low-frequency peak (the off-diagonal signal) is modulated as a function of the waiting time, while the high-frequency peak (the diagonal signal) remains nearly unchanged. In the non-rephasing spectra, the high-frequency peak (the diagonal signal) is modulated while the low-frequency peak (the off-diagonal signal) remains unchanged. This is the signature of quantum beat coming from two coupled oscillators, which are the symmetric and anti-symmetric carbonyl stretches in this case.

To further capture the quantum beating, time-domain non-rephasing data at waiting time of 1.5 ps are examined. Figure 7(a) depicts a trace at ω_t=2011 cm^{-1}. Clearly, a beating of two slow-varying oscillatory signals is shown, which indicates a pair of coupled vibrators. The period is roughly 760 fs, which corresponds to a frequency separation of ca. 44 cm^{-1}. This is what we observed in linear IR and 2D IR spectra for the symmetric and antisymmetric carbonyl stretches of $CpFe(CO)_2Cl$. On the other hand, the beating can also be reflected from pump-probe spectra. This is shown in Fig.7(b), where the magic-angle pump-probe kinetics is recorded at 2011 cm^{-1} up to 4.5 ps with delay step of 0.02 ps. Clearly, the beating shows the early stage of the pump-probe data. On the other hand, such a beating will not be easily observed in the 2D IR spectra of the reactant due to the ss-mode of the *cis* form that is located at the high-frequency side, and the as-mode of the *trans* form that is located at the low-frequency side. The as-mode of the *cis* form, however, is located very close to that of the *trans* form. There will be no beating between the *cis* and *trans* forms. But there will be some weak beating between the two modes of the *cis* form, because the transition intensity of the as/ss mode is quite weak. The assignment of these components can be found in Table II.

DOI:10.1063/1674-0068/26/06/721-728

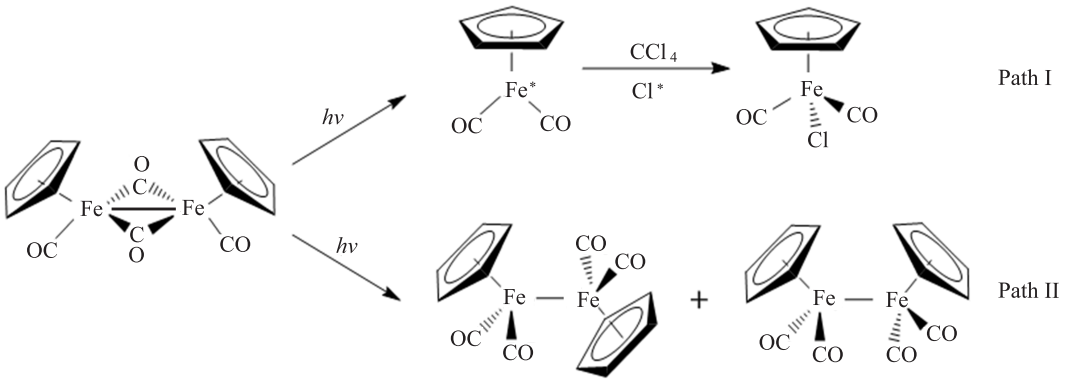

FIG. 8 Possible reaction pathways of $[CpFe(CO)_2]_2$.

F. Photoreaction of $[CpFe(CO)_2]_2$

$[CpFe(CO)_2]_2$ can generate two different photoproducts depending on the choice of UV pump wavelength excitation. Figure 8 shows the photochemical reaction pathways. The assignment of the photoproduct to $CpFe(CO)_2Cl$ (path I) rather than non-bridged $CpFe(CO)_2$ dimer (path II) because of the observed two equally strong IR transitions and the quantum beating between them. Also if it were non-bridged $CpFe(CO)_2$ dimer then the product with four terminal carbonyl groups (in *trans* and *gauche*-non-bridged forms) would have quite complicated IR signature [23]. In fact, the formation of $CpFe(CO)_2Cl$ has been observed previously [35], and its crystal structure has been reported [29]. We find that the photon energy of visible light is enough to cause hemolytic cleavage of the Fe−Fe bond, which leads to $CpFe^*(CO)_2$ radical. The formation of such radical has also been previously observed by irradiation with visible light [36]. The formed radical will further take a chloride from solvent to form a relatively stable species, $CpFe(CO)_2Cl$.

In addition, the observation of the beating and strong coupling in $CpFe(CO)_2Cl$ studied here resembles that seen in $Rh(CO)_2(C_5H_7O_2)$ system [21]. Here, sharing the same Fe atom causes an equally strong symmetric and antisymmetric C≡O stretching vibrations that are strongly coupled.

For the photoproduct, $CpFe(CO)_2Cl$, the antisymmetric, low-frequency mode is found to be more inhomogeneously broadened, as shown in the solid line in Fig.1. This could be due to the motion of the antisymmetric stretching vibration couples the motions of nearby solvent molecule in an antisymmetric way as well. Another reason is life time broadening effect. For this low-frequency component, the vibrational life time is roughly one third shorter than that of the high-frequency component, as observed by the pump-probe experiment (Table III).

IV. CONCLUSION

In this work, equilibrium photoproduct of π-cyclopentadienyliron dicarbonyl dimer $[CpFe(CO)_2]_2$ in nonpolar solvent CCl_4 has been investigated using one- and two-dimensional infrared spectroscopies. In CCl_4, the compound exists in both *cis* and *trans* isomers, with terminal carbonyl group facing on the same or different side of the Fe−Fe bond axis. One of the several possible photoreaction pathways of $[CpFe(CO)_2]$ dimer in CCl_4 is confirmed and the product shows a quantum beating time-resolved 2D IR spectra, between two equivalent transitions, which are found to be the antisymmetric and symmetric stretching of the terminal carbonyl stretching modes. The product was identified as $CpFe(CO)_2Cl$. This is the main product and its reaction pathway involves radial formation, follows chloride addition from solvent. Quantum-chemistry computations also support the proposed product. 2D IR spectra and the pump-probe results indicate that oscillations with a period of 0.76 ps consist with the peak splitting between the symmetric and antisymmetric carbonyl stretches. Our results indicate that 2D IR method can be readily used to differentiate the products of chemical reactions in condensed phases. This work also demonstrates why and when the vibrational beating would occur in multi-carbonyl group containing systems. Furthermore, intramolecular vibrational energy redistribution is found to occur between the antisymmetric and symmetric modes of the photoproduct. The rate constants are estimated to be on the order of tens of ps. In summary, the method presented in this work can be potentially used to monitor *in situ* molecular structure and dynamics of chemical species involved in solution-phase chemical reactions.

V. ACKNOWLEDGMENTS

The authors thank Prof. Zong-xiu Nie and Ms. Xue Yuan for ESI-mass spectroscopic measurement. This work was supported by the Knowledge Inno-

DOI:10.1063/1674-0068/26/06/721-728

vation Program (No.KJCX2-EW-H01), the Hundred Talent Fund from the Chinese Academy of Sciences, and the National Natural Science Foundation of China (No.91121020 and No.20727001).

[1] P. Hamm, M. Lim, and R. M. Hochstrasser, J. Phys. Chem. B **102**, 6123 (1998).
[2] M. C. Asplund, M. T. Zanni, and R. M. Hochstrasser, Proc. Natl. Acad. Sci. USA **97**, 8219 (2000).
[3] M. Khalil, N. Demirdoven, and A. Tokmakoff, J. Phys. Chem. A **107**, 5258 (2003).
[4] J. B. Asbury, T. Steinel, C. Stromberg, K. J. Gaffney, I. R. Piletic, and M. D. Fayer, J. Chem. Phys. **119**, 12981 (2003).
[5] C. Fang, J. Wang, A. K. Charnley, A. B. Smith III, S. M. Decatur, and R. M. Hochstrasser, Chem. Phys. Lett. **382**, 586 (2003).
[6] J. Wang, J. Chen, and R. M. Hochstrasser, J. Phys. Chem. B **110**, 7545 (2006).
[7] R. M. Hochstrasser, Proc. Natl. Acad. Sci. USA **104**, 14190 (2007).
[8] J. Bredenbeck, J. Helbing, R. Behrendt, C. Renner, L. Moroder, J. Wachtveitl, and P. Hamm, J. Phys. Chem. B **107**, 8654 (2003).
[9] J. Wang, J. Phys. Chem. B **111**, 9193 (2007).
[10] H. Maekawa, M. De Poli, C. Toniolo, and N. H. Ge, J. Am. Chem. Soc. **131**, 2042 (2009).
[11] A. D. Hill, M. C. Zoerb, S. C. Nguyen, J. P. Lomont, M. A. Bowring, and C. B. Harris, J. Phys. Chem. B (2013).
[12] C. R. Baiz, M. Reppert, and A. Tokmakoff, J. Phys. Chem. A **117**, 5955 (2013).
[13] Y. S. Kim and R. M. Hochstrasser, Proc. Natl. Acad. Sci. USA **102**, 11185 (2005).
[14] J. Zheng, K. Kwak, J. Asbury, X. Chen, I. R. Piletic, and M. D. Fayer, Science **309**, 1338 (2005).
[15] C. Kolano, J. Helbing, M. Kozinski, W. Sander, and P. Hamm, Nature **444**, 469 (2006).
[16] J. T. King, C. R. Baiz, and K. J. Kubarych, J. Phys. Chem. A **114**, 10590 (2010).
[17] J. T. King, J. M. Anna, and K. J. Kubarych, Phys. Chem. Chem. Phys. **13**, 5579 (2011).
[18] N. Demirdöven, M. Khalil, O. Golonzka, and A. Tokmakoff, J. Phys. Chem. A **105**, 8025 (2001).
[19] M. Khalil, N. Demirdöven, and A. Tokmakoff, J. Phys. Chem. A **107**, 5258 (2003).
[20] O. Golonzka, M. Khalil, N. Demirdöven, and A. Tokmakoff, J. Chem. Phys. **115**, 10814 (2001).
[21] M. Khalil, N. Demirdoven, and A. Tokmakoff, J. Chem. Phys. **121**, 362 (2004).
[22] J. F. Cahoon, K. R. Sawyer, J. P. Schlegel, and C. B. Harris, Science **319**, 1820 (2008).
[23] J. M. Anna, J. T. King, and K. J. Kubarych, Inorg. Chem. 50, 9273 (2011).
[24] W. Xiong, J. E. Laaser, P. Paoprasert, R. A. Franking, R. J. Hamers, P. Gopalan, and M. T. Zanni, J. Am. Chem. Soc. **131**, 18040 (2009).
[25] J. T. King, M. R. Ross, and K. J. Kubarych, J. Phys. Chem. B **116**, 3754 (2012).
[26] A. M. Woys, S. S. Mukherjee, D. R. Skoff, S. D. Moran, and M. T. Zanni, J. Phys. Chem. B **117**, 5009 (2013).
[27] P. A. Anfinrud, C. H. Han, T. Lian, and R. M. Hochstrasser, J. Phys. Chem. **95**, 574 (1991).
[28] R. H. Hooker, K. A. Mahmoud, and A. J. Rest, J. Chem. Soc., Chem. Commun. 1022 (1983).
[29] E. C. Johnson, T. J. Meyer, and N. Winterton, Inorg. Chem. **10**, 1673 (1971).
[30] F. Yang, Y. L. Liu, and J. P. Wang, Acta. Phys. Chim. Sin. **28**, 759 (2012).
[31] D. Li, F. Yang, C. Han, J. Zhao, and J. Wang, J. Phys. Chem. Lett. **3**, 3665 (2012).
[32] M. J. Frisch, G. W. Trucks, H. B. Schlegel, G. E. Scuseria, M. A. Robb, J. R. Cheeseman, J. T. Vreven, K. N. Kudin, J. C. Burant, J. M. Millam, S. S. Iyengar, J. Tomasi, V. Barone, B. Mennucci, M. Cossi, G. Scalmani, N. Rega, G. A. Petersson, H. Nakatsuji, M. Hada, M. Ehara, K. Toyota, R. Fukuda, J. Hasegawa, M. Ishida, T. Nakajima, Y. Honda, O. Kitao, H. Nakai, M. Klene, X. Li, J. E. Knox, H. P. Hratchian, J. B. Cross, C. Adamo, J. Jaramillo, R. Gomperts, R. E. Stratmann, O. Yazyev, A. J. Austin, R. Cammi, C. Pomelli, J. W. Ochterski, P. Y. Ayala, K. Morokuma, G. A. Voth, P. Salvador, J. J. Dannenberg, V. G. Zakrzewski, S. Dapprich, A. D. Daniels, M. C. Strain, O. Farkas, D. K. Malick, A. D. Rabuck, K. Raghavachari, J. B. Foresman, J. V. Ortiz, Q. Cui, A. G. Baboul, S. Clifford, J. Cioslowski, B. B. Stefanov, A. G. Liu, Liashenko, P. Piskorz, I. Komaromi, R. L. Martin, D. J. Fox, T. Keith, M. A. Al-Laham, C. Y. Peng, A. Nanayakkara, M. Challacombe, P. M. W. Gill, B. Johnson, W. Chen, M. W. Wong, C. Gonzalez, and J. A. Pople, *Gaussian 03, Revision B.05 Gaussian*, Pittsburgh, PA: Gaussian, Inc., (2003).
[33] S. T. Roberts, J. J. Loparo, and A. Tokmakoff, J. Chem. Phys. **125**, 084502 (2006).
[34] A. Ghosh and R. M. Hochstrasser, Chem. Phys. **390**, 1 (2011).
[35] T. S. Piper, F. A. Cotton, and G. Wilkinson, J. Inorg. Nuc. Chem. **1**, 165 (1955).
[36] L. R. C. Barclay and K. U. Ingold, J. Am. Chem. Soc. **102**, 7794 (1980).

DOI:10.1063/1674-0068/26/06/721-728